Fracture Behaviour of Brittle Plastic Sheets Containing Hollow or Embedded Stress Concentrators

——Interfacial Bonding Force and Fracture Behaviour——

By Akio TAKIMOTO*, Nobuo KUNIKI**, Yoshito YAMASHITA***, Masaki TAIDE**** and Noriaki USHIMOTO*****

(Received July 15, 1980)

Abstract

By introducing various hollow or embedded stress concentrators in the middle length of brittle plastic tensile sheet specimens, efforts have been made to investigate effects of these on design factors such as fracture strength, the superimposed stress concentration factor, the highest order fringe site, the fracture path including the fragmentation phenomenon and so on. Emphasis is directed toward the relationship between interfacial bonding force and fracture behaviour.

Introduction

Much work has been accomplished in theoretical and experimental researches on stress concentrations of plates having a various hollow stress raiser or a pair of these in a row which are in mutually apart away. Stress concentrations of a plate having a circular disk turn out to be very complicated since the interfacial bonding force between a disk and a matrix should take part in and fracture behaviour develops complexly. In the case that a matrix and a disk materials have different elastic constants, namely E_m and E_d, respectively and that the interface is perfectly bonded, Sezawa[1] and Saleme[2] have given theoretical solutions on stress distributions around the disk. In the case that the contact face of a circular disk is smooth and no shearing stress $\tau_{r\theta}$ would work there, Stippes[3] has given exact solutions of σ_θ and σ_r on a condition of E_m being equal to E_d. Chan[4] has also shown an approximate solution on that by using the F. E. M.. Hussain[5] has given exact solutions of σ_r and $\tau_{r\theta}$ for a similar problem where the interfacial bonding has some frictional force. All works mentioned above give solutions of stresses on/or around the interface and no work has so far been reported on the fracture strength and the fracture behaviour of plates having solid or embedded stress concentrators. Experimental programs on them have long been performed[6~12] and the viewpoint of interfacial bonding force and fracture behaviour is reported here.

* Department of Industrial Mechanical Engineering
** Graduate student, Industrial Mechanical Engineering
*** HIKARI WORKS, Nippon Steel Corporation
**** DAIHATSU KOGYO Co., LTD.
***** TAIHEI KOGYO Co., LTD.

Experimental Procedure

Thermosetting plastic sheets made of unsaturated polyester (U. P.) resin, Rigorac 1557C with additions of small amounts of the hardner, M. E. K. P. and the promoter, Cobalt-N become very brittle after a proper heat treatment. Before test programs start, smooth specimens and specimens having a large circular hole of this material were previously tested to fracture at room temperature to examine the brittleness of the material and the stress concentration factor of 3 which is the theoretical value for a circular-hole specimen and this material was found to be useful.

Test specimens having various stress concentrators such as a circular hole of different radius, a circular disk, two holes or disks in a row, three holes or disks in a row, edge notches and holes or disks and an inclined key-hole notch or cylindrical solid bar were prepared and tension tests were made on them to investigate the superimposed stress concentration factors by photoelastic methods, fracture strength, fracture behaviour such as fragmentation, fracture path and others.

Designs of some specimens are shown in Fig. 1. In specimens of the A series, the diameter of a hole was varied from 0.4 mm to 7.2 mm in five steps and from 1.5 mm to 24 mm in six steps for material thicknesses of 6 mm and 4 mm, respectively. In the B series, three different sets of three holes or disks of the same size (B1), two small ones and a large one (B2) and two large ones and a small one (B3) were designed and in each series the interflaw distances had four different values of 1.2, 3.8, 12.5 and 25 mm. The C series specimens, containing 15% depth U-notches at both edges, contained holes or disks in front of them at four different distances of 1.2, 3.6, 12 and 24 mm. In the D series specimens, a key-hole notch or a cylindrical

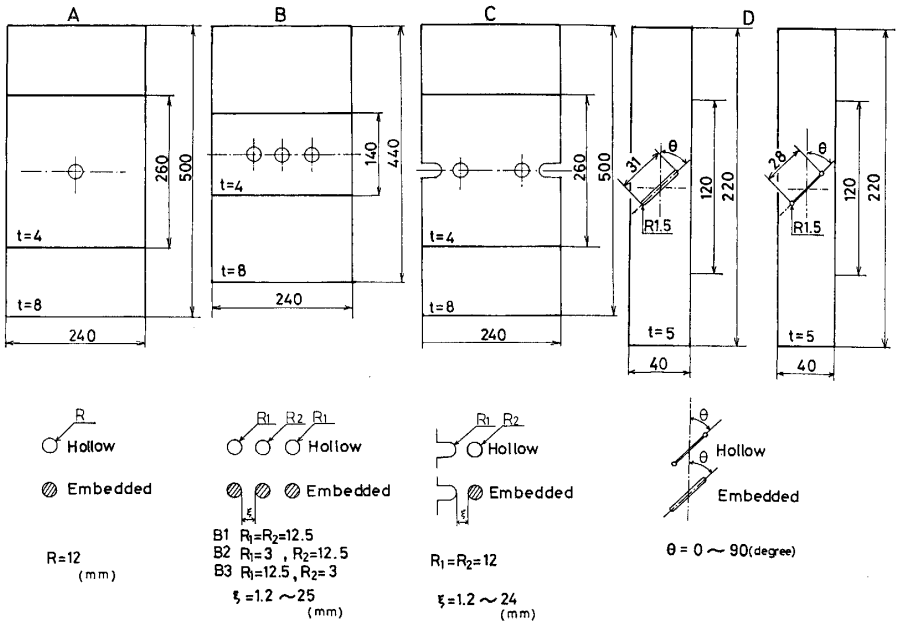

Fig. 1 Tension specimens having hollow or embedded stress concentrators.

solid bar was purposely inclined to the tensile axis in seven different angles from 0° to 90°.

All specimens were tested to fracture at room temperature by using Shimadzu Autograph IS–5000 machine and photoelastic photographs were taken at several different applied loads during the testing by covering the whole specimen with a proper bag not to miss any countable fragment.

Experimental Results

Theoretical elastic stress concentration factor K_t for a design having a circular hole is nearly 3[13] in a specimen whose width to the hole diameter ratio (W/D) is larger than 6. A question is brought here on the effects of the hole diameter beyond the W/D limitation mentioned above and the plate thickness on the fracture strength of a circular hole specimen. Green[14], Sternberg and Sadowsky[15] and Nakahara[16] have analytically given that the tensile stress becomes higher as it goes closer to the mid-thickness of a plate and this fact has also been verified by Rubayi[17] in photoelastic experiments and by Tan[18] in a boundary integral equation method. In Fig. 2, the effect of the hole diameter on fracture strength σ_f and stress concentration factor K_t is shown for specimens having a circular hole of various radii in two different plate thicknesses. Fracture strength increases and stress concentration factor decreases as the hole diameter decreases within a range of small diameters.

Figure 3 shows results of the specimens having an embedded stress concentrator in which the disk diameter is 24 mm where the plate thickness itself would not affect the stress concentration factor. Fracture initiates at angles between 40° to 90° to the tensile axis in contrast to the fact that it is usually confined to the very narrow region around the transverse axis in the case of a circular hole specimen. The initiation at less angle site mostly has happened at lower average fracture strength, namely an incipient

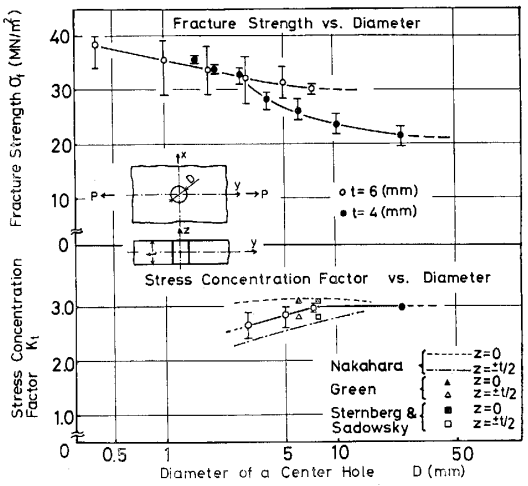

Fig. 2 Effect of hole diameter on fracture strength σ_f and the stress concentration factor K_t in specimens having a circular hole in cases of two different plate thicknesses.

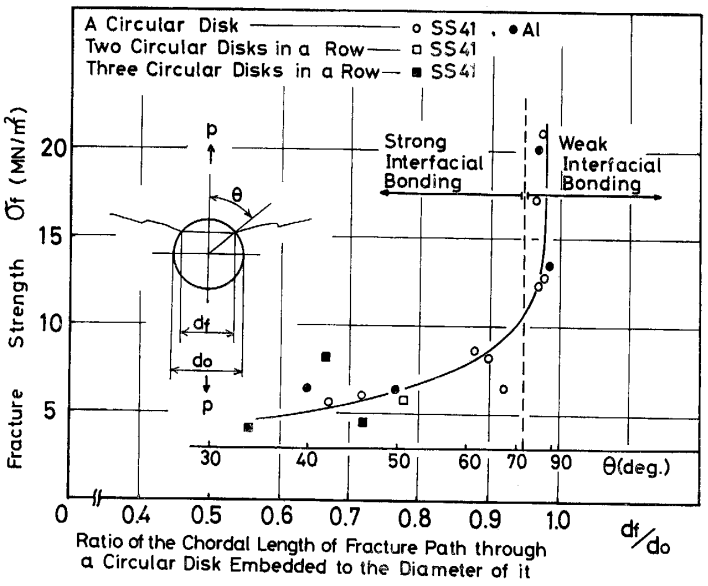

Fig. 3 Relationship between fracture strength and the ratio of d_f/d_0 in specimens having a central circular disk embedded.

fracture phenomenon which occurs often in a specimen having the strong interfacial bonding force between a metal disk and the plastic matrix. The strength of the interfacial bonding force seems to control the angle of an initiation site and may affect fracture strength of the specimen. These results indicate that the interfacial bonding condition plays a very important role in the study of fracture behaviour. A relationship between fracture strength and the ratio of d_f/d_0 (d_f: chordal length of fracture path through a disk, d_0: the diameter of a disk embedded) is also indicated in the figure.

Differences appeared in photoelastic fringe distributions around a hole and an embedded disk are compared in Photo 1. Photograph 1A for a circular hole shows the highest order fringes at both free boundaries on the transverse axis. Photograph 1B for an aluminum disk embedded shows the highest order fringes at some angles off above and below the transverse axis. This fact is also true for Photo 1C of a ferrous disk embedded. Photograph 1D shows an example of a strong interfacial bonding and

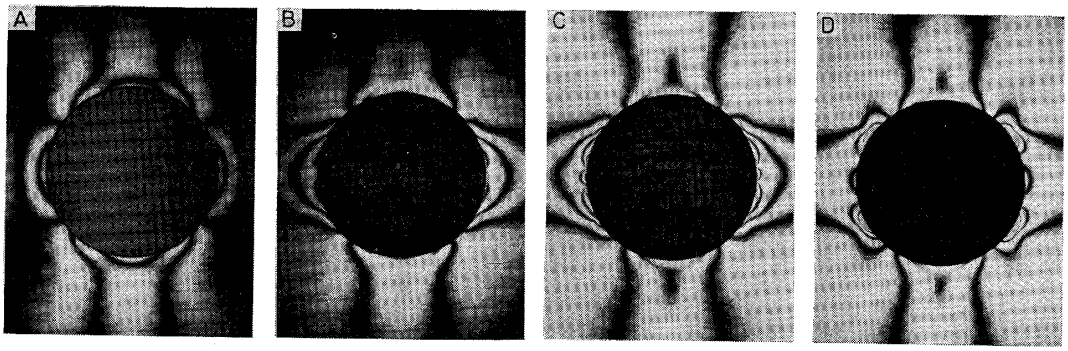

Photo 1 Photoelastic fringe patterns developed around a hole (A), a weakly bonded aluminum disk (B), a weakly bonded SS-41 disk (C) and a strongly bonded SS-41 disk (D) taken at a load of 8.2 MN/m².

more fringes appear at the same applied load and the highest order fringe sites shift upward and downward further compared to the previous ones of the weak bonding.

Variation of the highest order fringe site is shown as a function of the applied stress in Fig. 4 for weak and strong interfacial bonding tests. The highest order fringe site starts at lower angle and shifts to higher angle as average applied stress increases. The curves for the weak bonding appear in upwards in the figure compared to the ones downwards for the strong bonding. All three curves for the weak bonding indicate a value of 80 degree as an asymptote of them. Curves for the strong bonding hardly approach to this value. The order of the highest shear fringe observed certainly changes with the interfacial bonding condition. The incipient fracture occurs in the strong bonding condition and fracture is seemed to initiate at around the highest order fringe site. The site in a circular hole specimen is no doubt at zero degree and never shifts with an applied stress.

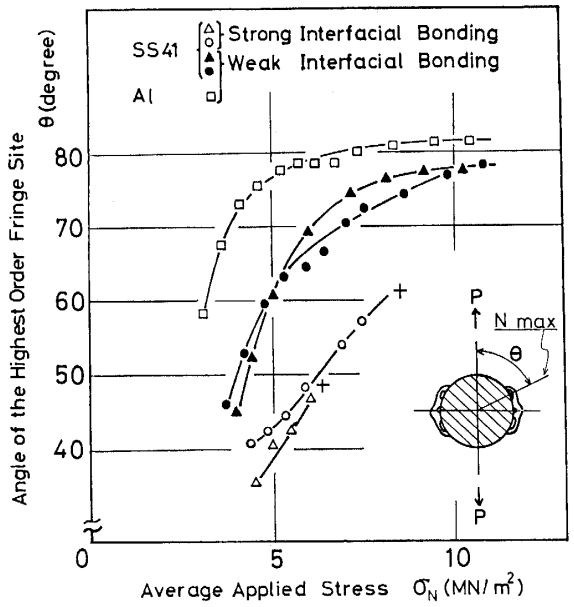

Fig. 4 Variation of the highest order fringe site as a function of applied stress for different interfacial bonding conditions.

Fracture strength and stress concentration factor for the specimens (B series) having three hollow or embedded stress concentrators in a row are shown in Fig. 5 (A and B). In comparing Fig. 5A to Fig. 5B, there can be found the relaxation effects in both fracture strength and the stress concentration factor. The relaxation effect in fracture strength becomes pronounced as the interflaw distance (ξ) decreases in different manners for all three indicated arrangements of disks. It is understood that all data indicate the weak interfacial bonding examples. Results for specimens having edge notches and holes or circular disks embedded are also given in Fig. 5 (C and D). In comparing Fig. 5C to Fig. 5D, relaxation effects are hardly observed for weak interfacial bonding tests in specimens having disks of aluminum and SS–41. Low fracture strength due to incipient fracture is again shown for specimens having SS–41 disks in

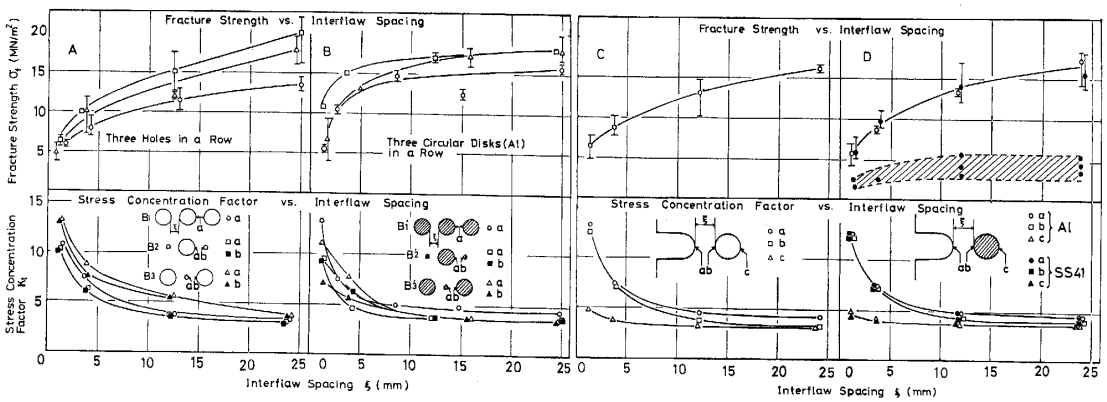

Fig. 5 Variations of fracture strength and stress concentration as functions of the interflaw spacing ξ in specimens having different arrangements of three holes (5A) or embedded disks (5B), edge notches and holes (5C) or circular disks embedded (5D).

the strong interfacial bonding condition. Differences in fringe developments in those specimens are shown in Photo 2. Photoelastic results taken at an applied stress about 10.2 MN/m^2 are given for the combination of an edge notch and a hole, having two different interflaw distances $\xi_1=24$ mm (photo 2A) and $\xi_2=3.6$ mm (photo 2B). Photographs 2C and 2D are results for an edge notch and a SS–41 disk. The differences in ways of appearing fringes and of developing them are clearly seen.

The relationships between fracture strength and the inclined angle of the stress concentrator to the axis of loading is indicated in Fig. 6. Results for an inclined key-hole notch are in Fig. 6A and are very similar to the one by Wilson[19] and Wu and co-workers[20]. Figure 6B gives the relationship for an inclined cylindrical solid bar. These two relations show a great difference in the influence of the inclined angle on fracture strength.

The differences appeared in photoelastic fringe distributions are compared for these in Figs. 7 and 8. Although the former taken at the net stress of 13 MN/m^2 and the latter at the load of 10 MN/m^2, the ways of appearing in these are directly comparable with.

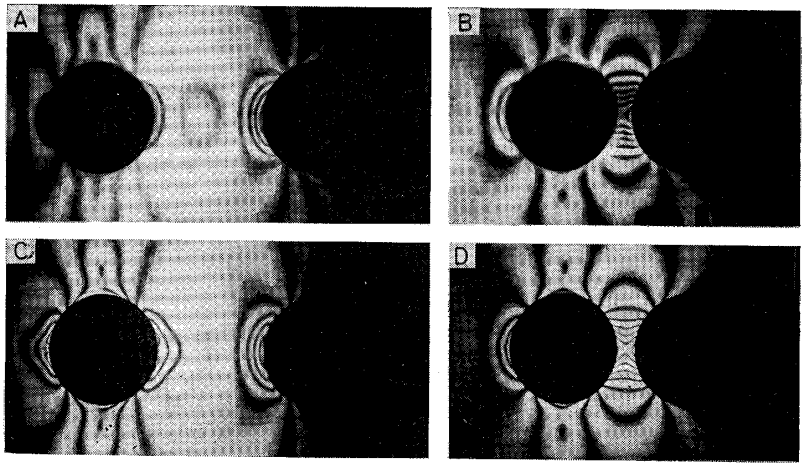

Notch & Circular Hole
A: $\sigma_{ave}=10.2$ MN/m^2
B: $\sigma_{ave}=8.1$

Notch & Circular Disk (SS–41)
C: $\sigma_{ave}=10.2$
D: $\sigma_{ave}=8.2$

Photo 2 Photoelastic fringe patterns developed in the zone of an edge notch and a hole (A, B) or an embedded disk of SS–41 (C, D) for two different interflaw distances of ξ.

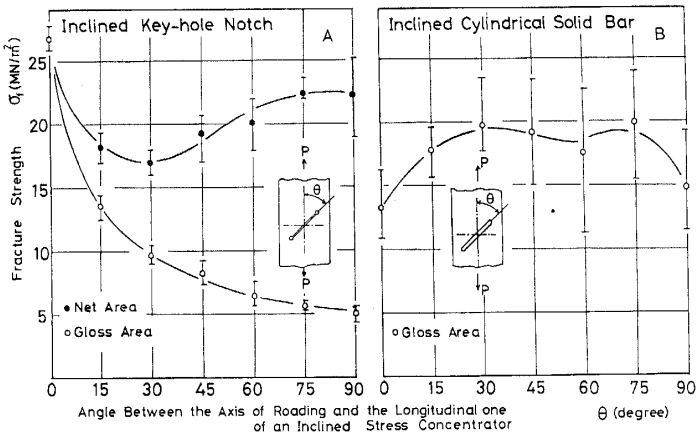

Fig. 6 Relationship between fracture strength and the inclined angle for specimens containing an inclined key-hole notch or cylindrical solid bar.

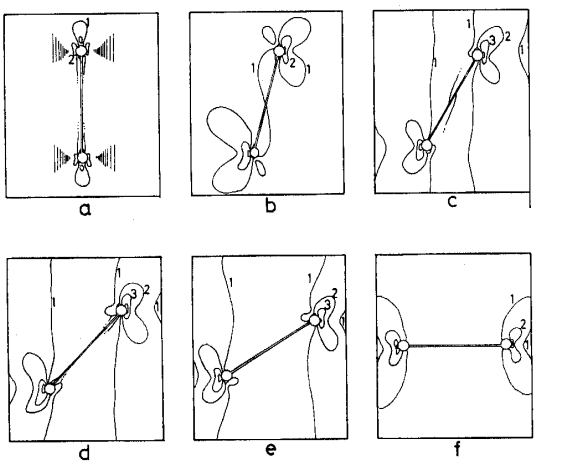

Fig. 7 Schematic fringe patterns obtained in photoelastic experiments for specimens having an inclined key-hole notch at net stress of about 13 MN/m².

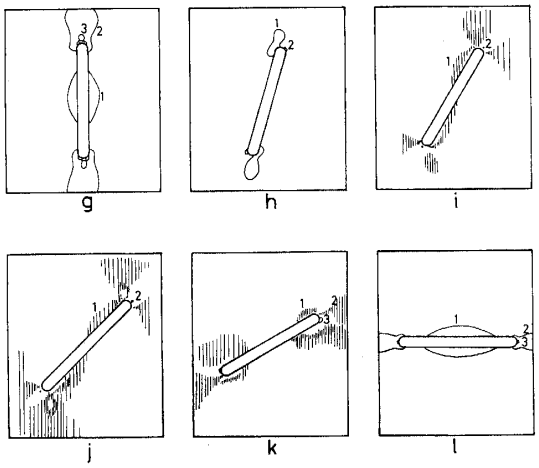

Fig. 8 Schematic fringe patterns obtained in photoelastic experiments for specimens having an inclined cylindrical solid bar at a load of 10 MN/m².

Variations of fracture paths are shown in Figs. 9, 10 and 11, due to factors such as a hole (Fig. 9A), a disk (Fig. 9B), notches and holes (Fig. 9D), notches and disks (Fig. 9E), the incipient fracture phenomena (Fig. 9, C and F), inclined angles of a key-hole notch (Fig. 10, a to f) and a cylindrical solid bar (Fig. 11, g to l). The extent of the fracture path is narrow in specimens having embedded stress concentrators and broad in ones having hollow stress concentrators. The extreme case of it becomes to be a sharp line as in specimens accompanied with incipient fracture (Fig. 9, C and F) and the fracture strength in this case is very low. Fracture initiates at the maximum stress concentration site in specimens having a key-hole notch and does not always so in specimens having solid bar due to the interfacial bonding condition.

The number of fragments in fracture are plotted to the fracture strength ratio in Fig. 12 as an example for specimens having three holes or disks (series B). The fact that the number of fragments for the latter (disk specimens) show lower values than the

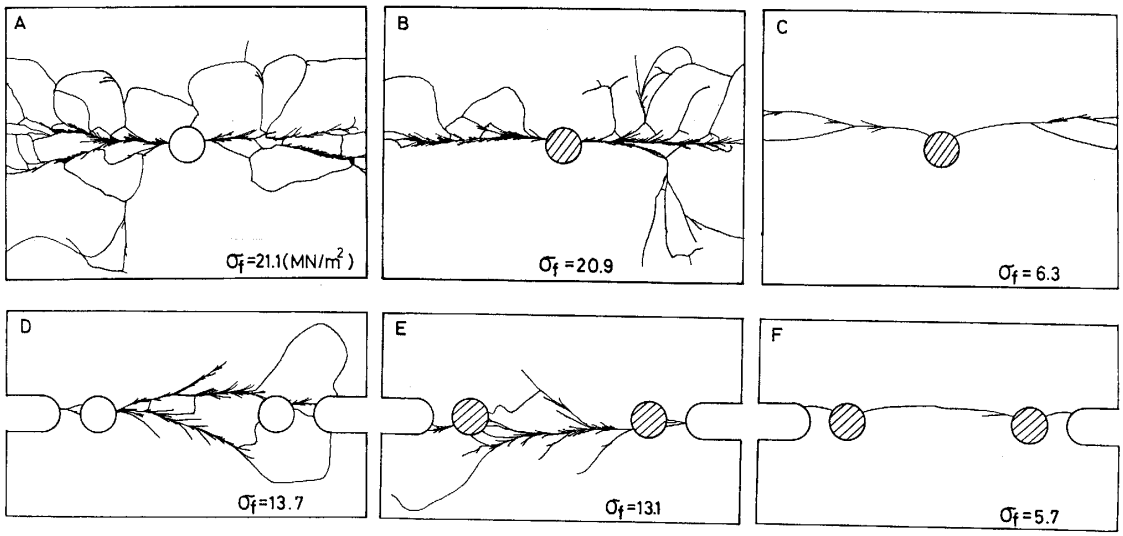

Fig. 9 Schematic presentations of fracture paths developed in specimens having a circular hole (9A), an embedded disk (9B, 9C), edge notches and holes (9D) and edge notches and embedded disks (9E, 9F).

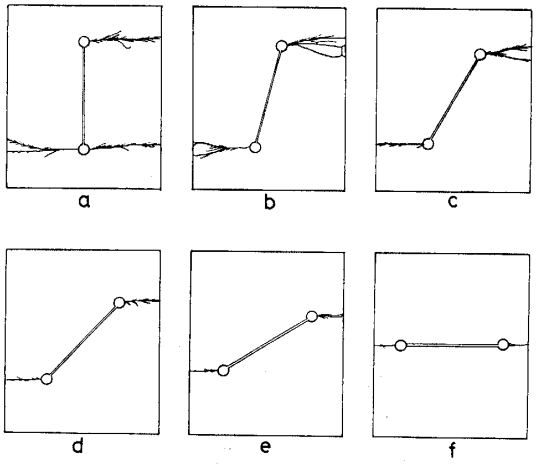

Fig. 10 Schematic presentations of fracture paths developed in specimens having an inclined key-hole notch.

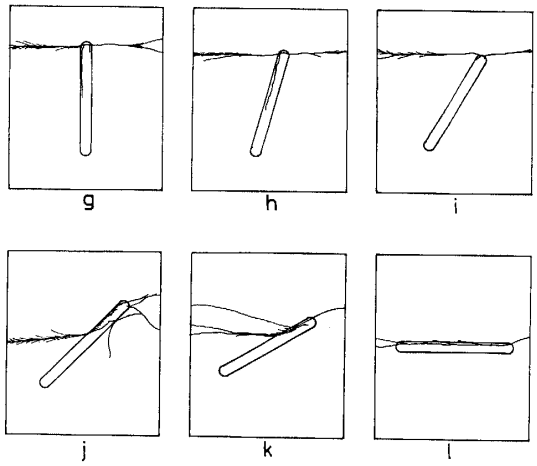

Fig. 11 Schematic presentations of fracture paths developed in specimens having an inclined cylindrical solid bar.

ones for the former (hole specimens) is in a good agreement with the differences appeared in the observation of the fracture path mentioned above. This agreement can also be proved in other examples of fracturing into fragments not presented here.

Discussion

Effort has been made to seek a clue to fracture mechanics of a material containing inhomogeneous second phases. Design of strength and the stress concentration factor of engineering brittle sheets containing macroscopic second phases of a different material is hardly made if the interfacial bonding force between them must be considered.

Brittle fracture strength of solid materials containing coherent or incoherent second phases of microscopic dimensions is hard to estimate since no information on the effect of the interfacial bonding condition on fracture has been available. Based on the results presented so far discussions are made here on the relations between the interfacial bonding force and the fracture behaviour of brittle sheet materials.

Interfacial Bonding Force and Fracture Strength

Fracture strength of a specimen having a circular hole of $\phi 24$ mm whose thickness is 4 mm approaches to a definite value of 20 MN/m^2 where the effect of the ratio of a hole radius to a plate thickness (r/t) is considered to be almost none and the stress concentration factor of it proves exactly this fact as shown in Fig. 2. Fracture strength of a specimen of the same dimensions with this except that a metal disk is embedded instead of a hole is lowered down to 5 MN/m^2 depending upon the interfacial bonding force acted as shown in Fig. 3. The stress concentration factor of this design, as it is easily compared with in Photo 1, shows larger value than 3 which is the theoretical one for a circular hole and it becomes larger as bonding force does stronger. The location of being maximum stress concentration is also influenced by interfacial bonding force. It starts on the transverse axis for the completely non-bonding condition such as a circular hole and rotates towards the axis of loading as bonding force increases as shown in Figs. 3 and 4 and in Photo 1. This can also be verified by the fact that stronger the bonding force, smaller the value of d_f/d_0 since the fracture initiates at the maximum stress site. Hussain[5] recently has given stress distributions of σ_r and $\tau_{r\theta}$ for an incomplete bonding condition. His model is very close to the one which this study has experimentally approached. The interfacial bonding region is divided into three classes of completely non-bonding, slipping and tight bonding as shown in Fig. 13. The first non-bonding region having the angle θ from 0° to η indicates that the primary bonding between a second phase and a matrix is broken under the applied tensile load of P. The second region, $\eta<\theta<\alpha$, shows slipping in between two surfaces due to the shearing component of the applied load. The last tight bonding region, $\alpha<\theta<\pi/2$, shows the complete interfacial bonding between contacted faces. Hussain has given that a maximum of σ_r on the transverse axis ($\theta=90°$) which is not altered by the coefficient of friction and a maximum of $\tau_{r\theta}$ works at the angle of α which is shifted towards the axis of loading as the coefficient of friction increases but the angle, α is independent of applied stress.

Figure 4 shows that the highest order fringe site shifts from 0 to 80 degrees depending on applied stress in contrast to the analytical results. If the elastic and plastic deformation contours of a hole in a plate under uniaxial tension is considered as given by Takimoto and co-workers[21,22], it is easily understood that the extents of angles for three different interfacial bonding conditions are varied by applied load and the highest order fringe site is naturally changed. The fact that weak bonding tests show the site at higher angle than that for strong bonding ones is in a good agreement with Hussain's results if the initiation of fracturing is assumed to be controlled by the shearing force acting on the interface since it may start on this surface. The propagation process is

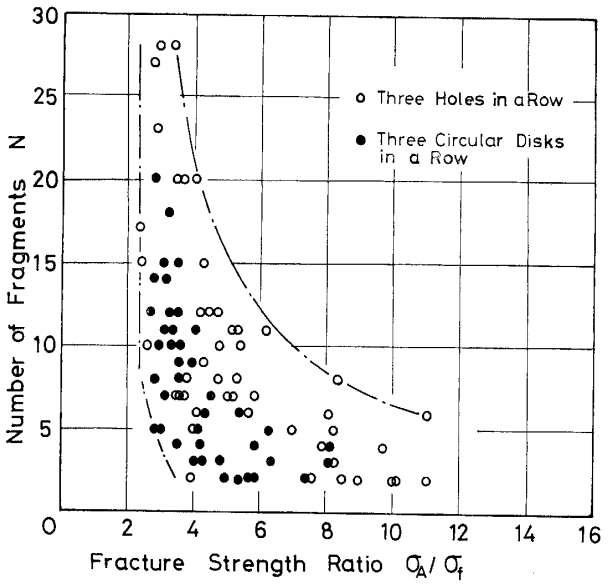

Fig. 12 Relationship between the number of fragments in fracture and the fracture strength ratio in the U.P. sheet material tested in tension.

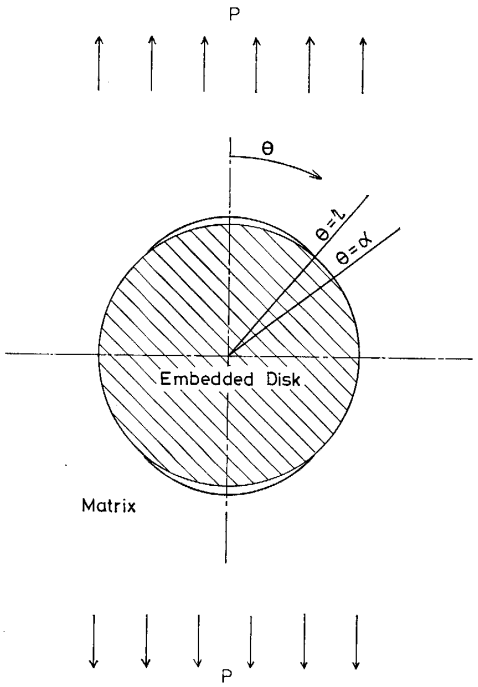

Fig. 13 A model showing three different interfacial regions of non-bonding, slip and tight bonding.

of course controlled by the tangential force σ_θ. Such an example of the shifted initiation and sharp propagation is clearly demonstrated in Fig. 9C.

Stippes and co-workers[3] have given the maximum stress concentration factor of 2.75 for a circular embedded disk with non-interfacial shearing force in the case of $E_{\text{matrix}}=E_{\text{disk}}$ where E's are Young's moduli. This value is smaller than 3 and is seemed to have an effect of relaxation. The case of non-interfacial bonding assumed, similar effects of relaxation are experimentally obtained in Fig. 5B where fracture strength shows higher values and stress concentration factors do lower values than those given in Fig. 5A at smaller interflaw distances. In the design having edge notches and disks introduced in Fig. 5D edge notches work as a main stress concentrator and the relaxation effect is hardly recognized experimentally. In the case having a cylindrical solid bar, fracture strength as shown in Fig. 6 depends on the interfacial bonding condition complexly in addition to factors due to its geometrical location in three dimensions as its fringe developments can be seen in Fig. 8. These interfacial and geometrical factors must be solved in future.

Interfacial Bonding Force and Fracture Behaviour

Most of specimens fractured in fragments in tension where the number of fragments were differed widely from one specimen to another depending upon fracture strength as shown in Fig. 12. In propagating a fracture by developing various fracture paths as examples in Figs. 9, 10 and 11, the surface energy U_S of creating fresh solid surfaces

and the kinetic energy U_K to propagate and to scatter the fragments away are required in addition to the elastic strain energy U_E. Accordingly the energy absorbed to fracture should be depend on fracture behaviour such as the number of fragments, the fracture path and so on. Such a relation is obtained for specimens having edge notches and holes or disks in Fig. 14 where the absorbed energy varies in parabolic fashion with respect to the area created in fracture.

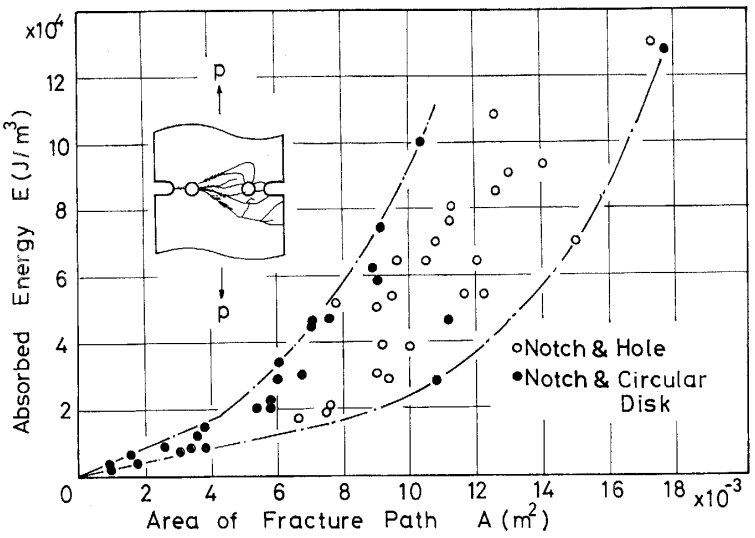

Fig. 14 Relationship between the absorbed energy and the area of a fracture path in the U.P. sheet material tested in tension.

Fracture at first initiates and then propagates. Two processes are considered in the propagation. A crack runs perpendicular to the normal stress with linear fashion in the primary fast propagating process and results in the subsequent fast process in branching off the crack with multiple hangnails. In the final moment of the primary process, the energy of the total system is given by

$$U = -U_E + U_S \qquad \cdots\cdots\cdots(1)$$

where U : energy given by the external system
U_E : elastic energy stored in a specimen
U_S : surface energy of creating fresh surfaces (crack).

Before fracture initiates U_S is zero and U is equal to $-U_E$, all energy is stored in a specimen which is given by $V\int_0^{\varepsilon}\sigma d\varepsilon$. In fracturing, U_E presents a certain value which is a function of a crack length and the surface energy retains the rest of the energy. In the subsequent fast fracture, however, an equilibrium in Eq. (1) may not be correct since the kinetic energy should be added due to Newton's law of motion and is given by

$$U = -U_E + U_S + U_K \qquad \cdots\cdots\cdots(2)$$

where U_K: kinetic energy in propagation and in scattering the fragments away.

The results in Fig. 14 show two stages in experimental curves. In the first stage

where the energy absorbed is low and the fresh surface created is a little, it seemed to complete fracture in the primary fast process only and the derivative of the energy with respect to the area created (dE/dA) is a constant which may be close to the value of the surface energy. In the second stage the energy absorbed is increased in parabolic fashion with the area of the fracture path. The subsequent fast process takes part in and the energy due to the kinetic component U_K should be added to those according to Eq. (2). This kinetic component increases as the total absorbed energy increases, that is, as the fracture strength increases. These results conclude that a design fractures at lower strength in the primary fast process with a propagation in a sharp line by creating less fresh area or fractures at higher strength in the subsequent fast process which should be influenced strongly by the kinetic energy in branching off cracks with multiple hangnails.

Conclusions

Based on results and discussion given so far the following items are concluded in regard to the relationships between interfacial bonding force and the fracture behaviour of brittle plastic sheet materials having hollow or embedded stress concentrators.

(1) The site of the maximum stress concentration is off the transverse axis and it changes with applied stress and also with the interfacial bonding condition in a design having an embedded disk in tension. The site rotates towards the axis of loading as bonding force increases.

(2) Incipient fracture takes place in a design of strong interfacial bonding and the fracture initiation point shifts towards the axis of loading in decreasing the ratio of d_f/d_0.

(3) A fracture path results in a sharp line in the case of low energy absorbed and runs in branching off with multiple hangnails in the case of high absorbed energy where the kinetic energy plays an important role.

(4) The way of shear fringe development essentially differs in the quasi-two dimensional stress concentrator of a key-hole notch and in the three dimensional embedded one, but the crack tends to propagate the minimum path in both cases.

References

1) Sezawa, K., Rep. Aero. Res. Inst. Tokyo Imp. Univ., **6** [68] 25 (1932).
2) Saleme, E. M., Appl. Mech., **25**, 129 (1958).
3) Stippes, M., Wilson, Jr. H. B. and Krull, F. N., Proc. 4th U.S. Nat. Cong. Appl. Mech., **2**, 799 (1962).
4) Chan, S. K. and Tuba, I. S., Int. J. Mech. Sci., **13** [7], 615 (1971).
5) Hussain, M. A. and Pu, S. L., J. Appl. Mech., **38**, 627 (1971).
6) Takimoto, A. and Yamashita, Y., Proc. Symposium Japan Soc. Mech. Eng., Lecture Meeting No. 775-2 (1977) (in Japanese).
7) Takimoto, A., Yamashita, Y. and Tanaka, H., Proc. Symposium Japan Soc. Mech. Eng., Lecture Meeting No. 788-3 (1978) (in Japanese).

8) Yamashita, Y., M. S. Thesis, Yamaguchi University (1979) (in Japanese).
9) Kuniki, N., B. S. Thesis, Yamaguchi University (1979) (in Japanese).
10) Takimoto, A., Kuniki, N. and Fujisawa, T., Proc. Symposium Japan Soc. Mech. Eng., Lecture Meeting to be presented in September, 1980 (in Japanese).
11) Ushimoto, N., B. S. Thesis, Yamaguchi University (1980) (in Japanese).
12) Taide, M., B. S. Thesis, Yamaguchi University (1980) (in Japanese).
13) Howland, R. C. J., Roy. Soc. London (A), **229**, 67 (1929).
14) Green, A. E., Roy. Soc. London (A), **240**, 69 (1948).
15) Sternberg, E. and Sadowsky, M. A., J. Appl. Mech., **16**, 27 (1949).
16) Nakahara, I., Trans. Japan Soc. Mech. Eng., **25**, 181 (1959) (in Japanese).
17) Rubayi, N. A. and Yadava, V., J. Strain Analysis, **8** [3], 220 (1973).
18) Tan, C. L. and Fenner, R. T., J. Strain Analysis, **13** [4], 213 (1978).
19) Wilson, W. K., J. Basic Eng., **93**, 685 (1971).
20) Wu, H. C., Yao, R. F. and Yip, M. C., J. Appl. Mech., **44**, 455 (1971).
21) Takimoto, A., Nai, M. and Inatomi, T., Memoirs of the Faculty of Eng., Yamaguchi Univ., **30** [2], 305 (1980) (in Japanese).
22) Takimoto, A. and Nai, M., Proc. Symposium Japan Soc. Mech. Eng., Lecture Meeting No. 805 –1 (1980) (in Japanese).